Title	III-nitride Light-emitting Diode with Embedded Photonic Crystals
Author(s)	LI, KH; ZANG, KY; CHUA, SJ; Choi, HW
Citation	Applied Physics Letters, 2013, v. 102, p. 181117
Issued Date	2013
URL	http://hdl.handle.net/10722/189022
Rights	Creative Commons: Attribution 3.0 Hong Kong License

III-nitride light-emitting diode with embedded photonic crystals

K. H. Li,[1] K. Y. Zang,[2] S. J. Chua,[2] and H. W. Choi[1,a)]
[1]*Department of Electrical and Electronic Engineering, The University of Hong Kong, Hong Kong*
[2]*Institute of Material Research and Engineering, Singapore*

(Received 27 December 2012; accepted 28 April 2013; published online 10 May 2013)

A photonic crystal has been embedded within an InGaN/GaN light-emitting diode structure via epitaxial lateral overgrowth of a p-type GaN capping layer. The photonic crystal is a hexagonal-closed-packed array of nano-pillars patterned by nanosphere lithography; the capping layer planarizes the disconnected pillars to form a current-injection device. Optical properties of the nanostructures and devices are extensively studied through a range of spectroscopy techniques and simulations. Most significantly, the emission wavelengths of embedded photonic crystal light-emitting diodes are nearly invariant of injection currents, attributed to partial suppression of the built-in piezoelectric in the quantum wells. © *2013 AIP Publishing LLC*. [http://dx.doi.org/10.1063/1.4804678]

The efficiencies of III-nitride light-emitting diodes (LEDs) have exceeded those of gas-discharge fluorescent lamps, although not to the extent LEDs are theoretically capable of. Quantum efficiencies fall short of their potentials, owing to a combination of factors: (1) the built-in piezoelectric field, a consequence of compressively strained InGaN/GaN quantum well layers, reducing internal quantum efficiency (IQE) due to non-optimal overlap between electron-hole wavefunctions;[1] (2) total internal reflections (TIR) due to the high refractive index contrast at the semiconductor/air interface, giving light extraction efficiencies of below 10%.[2] Reabsorption of confined photons generates heat, further jeopardizing IQE. A variety of solutions have been proposed to alleviate these issues. For example, growth on GaN substrates[3] offers the perfect solution to lattice-matched epitaxy eliminating strained-induced effects. On the other hand, structuring of LED chips at the nano-,[4] micro-,[5] and macro-[6] scales promotes light extraction by minimizing occurrences of TIR. At the nano-scale, the integration of photonic crystal (PhC) has been demonstrated to effectively improve optical performance and emission directionality. Although PhCs can be of the form of arrays of air-holes or pillars, works reported in the literature mostly adopt the former configuration.[7,8] Nevertheless, periodic arrays of pillars are not only equally capable of extracting guided photons but can potentially enhance IQE simultaneously through partial strain relaxation. Having said that, establishing electrical injection to an array of isolated nano-scale emitters is by no means an easy feat. Typically, electrical interconnection over a non-planar surface involves planarization via gap-filling[5] followed by chemical-mechanical polishing. Although feasible, filling up the air-gaps between adjacent nano-pillars reduces the refractive index contrast, disrupting optical properties of the PhC. In this work, an innovative approach of planarization through wafer regrowth is reported. A nanostructured device comprising a pillar-type PhC is planarized through the regrowth of a continuous p-doped contact layer. Such an overgrowth technique produces epitaxial layers with reduced threading dislocation densities and thus high crystalline quality.[9] With regards to the patterning of the nano-scale pillar array, nanosphere lithography (NSL) is adopted in this work, defining large-area hexagonal closed-packed patterns.

The LED wafer used in this study consists of $In_{0.2}Ga_{0.8}N$/GaN quantum wells (QWs) grown by metal-organic chemical vapor deposition (MOCVD) on a c-plane sapphire substrate. Silica nanospheres with mean diameters (d) of 192, 310, and 500 nm are used to assemble hexagonal closed-packed monolayers, serving as masking layers, the patterns of which are subsequently transferred to GaN by dry etching. Details of the NSL process has been described in Ref. 10. A continuous p-doped GaN layer is grown over the nano-patterned surface by epitaxial lateral overgrowth (ELO), also by MOCVD. The 300-nm thick p-type GaN ELO layer is grown at a temperature of 1070 °C and at a pressure of 60 Torr. A mixture of N_2 and H_2 is used as the carrier gas, while TMGa, Cp_2Mg, and NH_3 are the Ga, dopant, and N sources, respectively. The growth temperature is subsequently decreased to 800 °C whilst maintaining a N_2 ambient for 30 min to activate the Mg dopants. A Ni/Au (10 nm/10 nm) current spreading layer is deposited over the p-GaN ELO layer by electron-beam evaporation, followed by contact alloying at 600 °C in an oxygen ambient. The LED mesa regions with areas of $400 \times 200\ \mu m^2$ are defined by photolithography and dry etched to expose the n-GaN layer. Another photolithographic process is employed to define the p-pad and n-pad regions for contact metallization. A bilayer of Ti/Au (40/200 nm) is e-beam evaporated, followed by annealing at 550 °C in N_2 for 5 min to form ohmic contacts. The chips are diced by laser micromachining and mounted onto TO-headers for wire-bonding. A Spectra Physics 349 nm diode-pumped solid state (DPSS) pulsed laser is used as an excitation source for photoluminescence (PL) studies of the PhCs. The PL signals are dispersed by an Acton SP2500A 500 mm spectrograph and detected by a PI-PIXIS TE-cooled charge-coupled device (CCD), giving spectral resolutions of ~0.3 meV.

The schematic diagram in Fig. 1(a) highlights the key features of the device with embedded PhC. Planar and cross-sectional views of the embedded nanostructure is captured by field-emission scanning electron microscopy (FE-SEM, Hitachi S-4800) as shown in Figs. 1(b) and 1(c), clearly

a)Author to whom correspondence should be addressed. Electronic mail: hwchoi@hku.hk. Tel.: (852) 28592693. Fax: (852) 25598738.

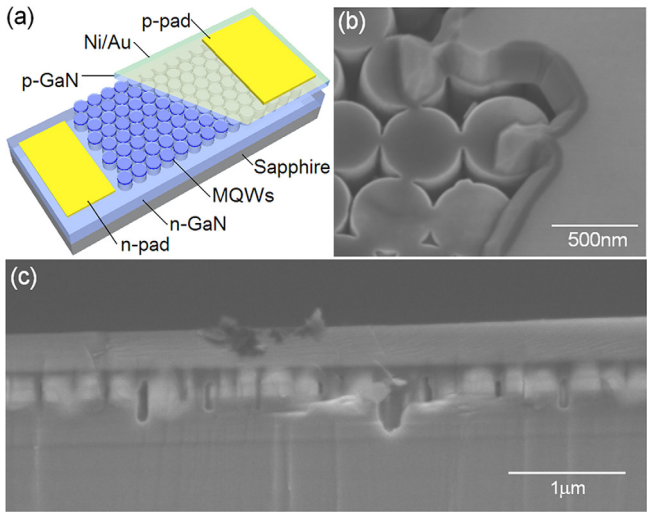

FIG. 1. (a) Schematic diagram showing the structure of an LED with embedded PhC; FE-SEM images showing (b) the edge region of the ELO regrown GaN layer covering the nanopillar array and (c) cross-sectional view the nanopillars planarized by the ELO layer.

revealing that the nano-pillars have been planarized by the ELO layer, leaving the air-gaps intact. The electrical, optical, and structural properties of the packaged devices are comprehensively characterized, complemented by finite-difference time-domain (FDTD) simulations for the optical properties of the PhC structure, as well as finite element strain simulations to illustrate the role of strain relaxation.

The enhancement ratios of the integrated PL signal for the PhCs before and after ELO, compared with the as-grown, are plotted in Fig. 2(a). The PL intensity is raised by as much as ~1.9 for $d = 192$ nm; the factor decreases with increasing d. Such closed-packed pillar arrays do not possess photonic bandgaps in the visible region; instead they operate as "weak" PhCs due to folding of dispersion curves of Bloch modes at the Brillouin zone boundaries.[11] The enhancement effects are weakened with insertion of the ELO layer, attributed to absorption. The PL spectra of the PhCs after regrowth, plotted in Fig. 2(b), reveal spectral blue-shifts as d decreases, tentatively attributed to strain relaxation.

The optical characteristics of the PhC with and without the ELO layer are further studied through 3-D FDTD simulations. The QWs are modeled as light sources inserted within each pillar, as illustrated in the diagrams depicted in Figs. 3(a) and 3(b). In the simulation, the propagation of

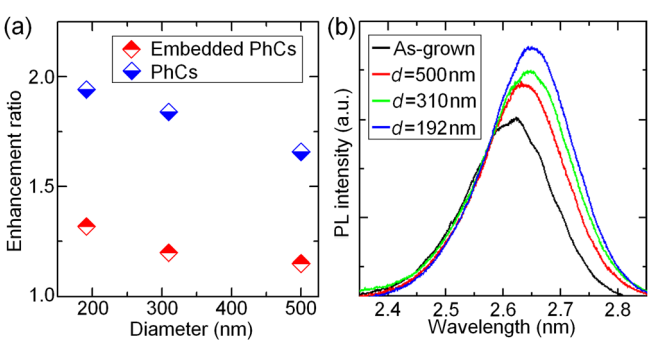

FIG. 2. (a) Enhancement ratios of the integrated PL signals for the PhCs before and after ELO growth; (b) PL spectra of the PhC after regrowth, together with that of the as-grown.

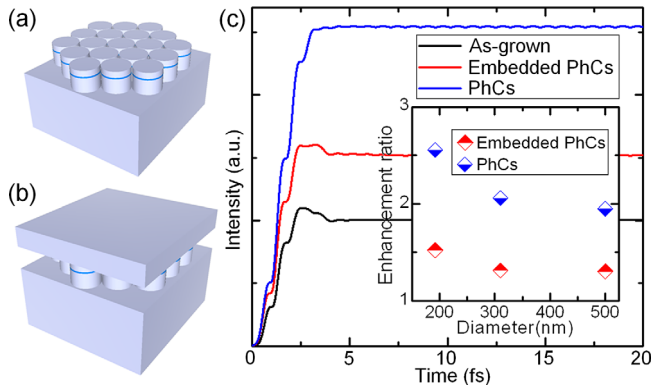

FIG. 3. Models of the (a) nanopillar PhC and (b) PhC after ELO regrowth used in the 3-D FDTD simulations. (c) Simulated results showing the light output intensities over time for the PhC LEDs before and after ELO regrowth, as well as for the as-grown LED. The data are summarized in the inset of the figure.

waves from the sources is detected and analyzed with a wide-field planar monitor placed on the top of the device models. The simulated data are plotted in Fig. 3(c), also summarized in its inset. Consistent with the measured PL data, insertion of the ELO layer does reduce light extraction probabilities but light output remains above as-grown levels. It is also noted that the simulated enhancement factors are, on average, 15% higher than the measured values.

The transmission characteristics of the PhC may be diminished by the presence of defects within the pillar array, a common feature of self-assembly techniques including NSL. Dimensional non-uniformities amongst spheres give rise to point defects as illustrated in the inset of Fig. 4(a). The role of imperfections in the PhC on its optical properties is investigated through additional simulations, conducted using modified models containing pillars with diameter deviations (σ) of $\pm 2.5\%$, $\pm 5\%$, and $\pm 7.5\%$ from the nominal value of 192 nm. The simulated results, as shown in Fig. 4(a), show that imperfect PhCs extract as much as 20% less light compared to perfect arrays. Since the diameters of the nanospheres used in this work are known to have deviations of up to $\pm 7.5\%$, the observation of lower-than-predicted PL intensities is justified.

Micro-Raman spectroscopy is employed to detect strain in the nano-pillars. The 325 nm line of a He-Cd laser, with shallow penetration in GaN, is chosen for Raman excitation so that the signals originate from the near-surface region. The spectral resolution of the setup is $\sim 0.2\,\mathrm{cm}^{-1}$. Raman spectra of the PhCs after regrowth showing the E_2(high) phonon mode, corresponding to lattice vibrations perpendicular to the surface (which is known to be sensitive to strain[12]), is plotted in Fig. 4(b). The degree of stress can be estimated with $\Delta\omega_{E2} = K_R\sigma$, where σ is the in-plane biaxial stress, $K_R (= 4.2\,\mathrm{cm}^{-1}\,\mathrm{GPa}^{-1})$ is the proportionality factor, and $\Delta\omega_{E2}$ is the shift of the E_2(high) phonon peak with respect to strain-free GaN, obtained as $567.5\,\mathrm{cm}^{-1}$ from a free-standing GaN wafer. The typical GaN epilayer exhibits large stresses due to mismatches in both the lattice constants and thermal expansion coefficients of GaN and sapphire. By patterning the GaN surface into nanopillars, a Raman shift ($\Delta\omega_{E2}$) of $0.8 \pm 0.2\,\mathrm{cm}^{-1}$ is observed for $d = 192$ nm, corresponding to residual stress of 0.35 ± 0.05 GPa. Strain

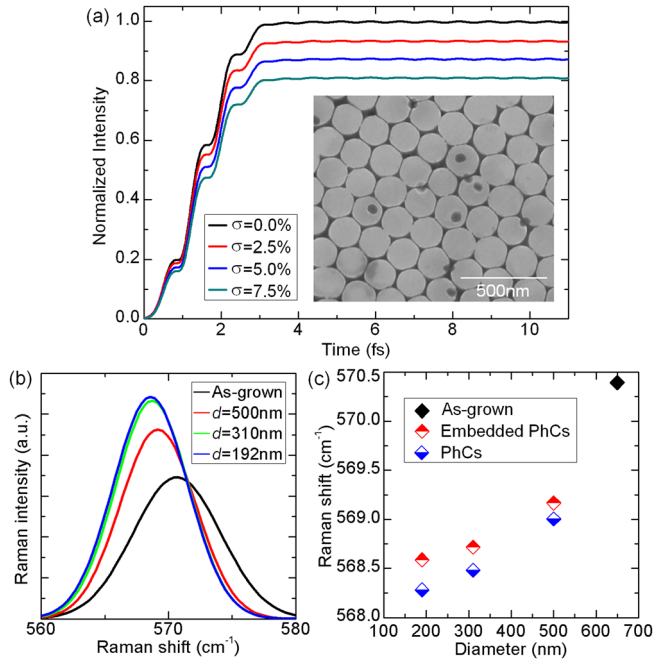

FIG. 4. (a) Simulated light output vs. time for the imperfect PhCs with various dimensional deviations; a FE-SEM image of the d = 192 nm nanopillar is shown in the inset, whereby defects caused by dimensional non-uniformity (σ) amongst nanospheres are seen; (b) Raman spectra for the PhC (after ELO) and the as-grown showing the E_2(high) phonon mode; (c) Plot of the Raman E_2(high) phonon mode frequency for the nanopillar PhCs of varying diameters.

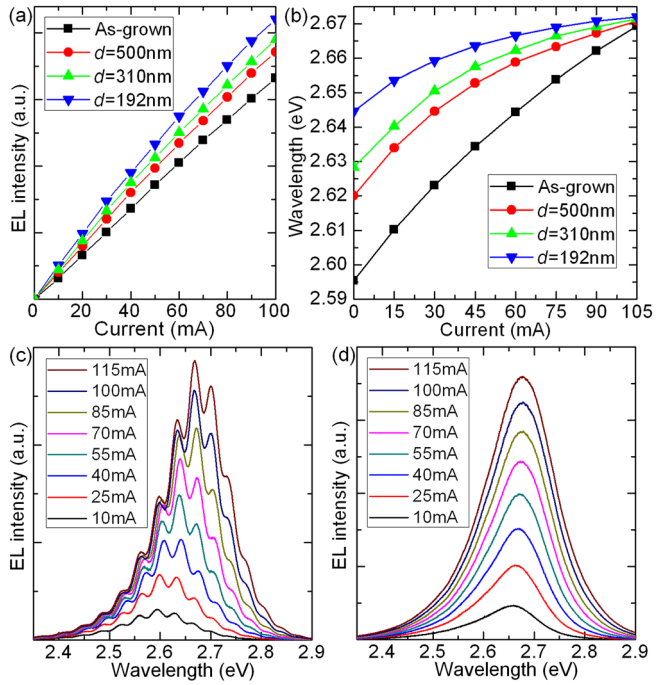

FIG. 5. (a) Plot of light output power as a function of injection current. (b) Plot of peak emission wavelength as a function of injection current. Room temperature EL spectra of an (c) as-grown LED and (d) LED with embedded PhC (d = 192 nm) operated at currents between 10–115 mA.

relaxation occurs mainly in the vicinity of surfaces as the surface atoms are less constrained by surrounding materials. Pillars of small diameters have high surface area to volume ratio, thereby increasing the extent of strain relaxation. Raman measurements are also conducted on an identical set of nano-pillar structures before ELO regrowth; the results are summarized in Fig. 4(c). A slight reduction of red-shift is observed from samples after ELO regrowth, signifying that the ELO cap layer is lightly strained (albeit much less than the as-grown). After all, ELO is a growth technique originally developed for achieving high-quality epilayers.

With the growth of a cap layer bridging isolated pillars, it becomes possible to inject currents into devices with the embedded PhCs. Fig. 5(a) plots electroluminescent (EL) output powers of the LEDs vs. injection currents. The LEDs with embedded PhCs emit as much as 20% more light over the un-patterned counterparts. Since a majority of photons emitted from the QWs are trapped within the device due to TIR, they would eventually be re-absorbed or escape from the sidewalls. On the other hand, the embedded PhC is capable of altering the directionalities of propagating photons. Thus, the overall enhancement of light extraction can be attributed to diffraction and scattering caused by the periodic change of refractive index in the PhC.

The emission center wavelength of an InGaN LED not only depends on the bandgap energy of the QW but is also strongly affected by the large piezoelectric field arising from the built-in strain. The triangular-shaped potential well caused by the piezoelectric field and spontaneous polarization tilts the band alignment separating the electron and hole wavefunctions, causing spectral red-shifts and reduction of radiative recombination rates. To determine dimensional effects on the emission spectrum, the LEDs are driven in pulsed mode (1 μs, 1 kHz) to minimize self-heating effects. The emission spectra of the as-grown LED in Fig. 5(c) indicate significant blue-shifts of ~74 meV as the bias currents increase from 10 to 115 mA. With increasing currents, the injected carriers partially screen the polarization field; such screening re-shapes the potential function back to a rectangular profile, leading to the observed spectral blue-shift. The filling of localized states in the well and barrier layers may yet be another factor leading to the reduction of effective carrier separation. However, a gradual saturation of localized states would lead to a reduction in quantum efficiency caused by enhanced capture rates by non-radiative recombination centers. The L-I data in Fig. 5(a) indicate that the LEDs maintain nearly linear increases in light emission at higher injection currents. In view of this observation, the spectral blue-shifts are mainly attributed to the screening of the polarization field. The emission spectra for the PhC LED (d = 192 nm) are plotted in Fig. 5(d); it is observed that the peak wavelength is nearly invariant of driving currents, signifying that the strain effect is significantly diminished. The spectra are also characterized by the lack of interference fringes as compared to the as-grown, indicating that Febry-Pérot oscillations have been effectively suppressed by the embedded PhC. A plot of peak wavelength with respect to bias currents for the LEDs is shown in Fig. 5(b). As d shrinks from 500 to 192 nm, the extent of spectral blue-shift reduces from 50 to 27 meV over the current range of 10 to 115 mA, compared to a 74 meV spectral shift of the as-grown LED over the same current range. Such observations of diminishing blue-shifts clearly attest to the role of strain relaxation through nano-structuring.

A 3-D simulation has also been performed employing finite element approach to map strain distributions along the

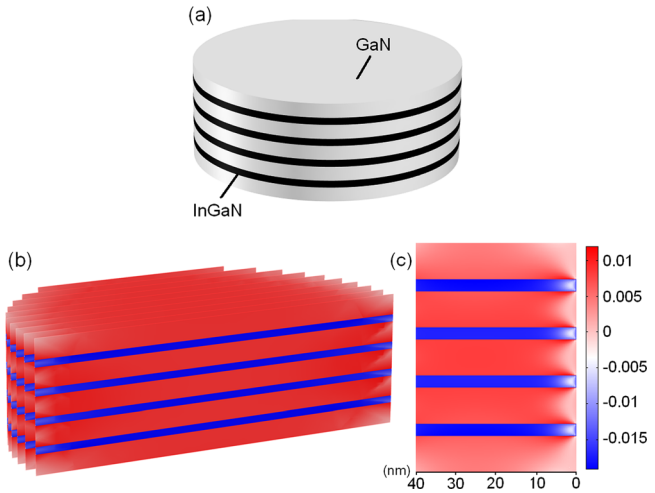

FIG. 6. (a) The disk model containing four pairs of InGaN/GaN QWs as used in the 3-D finite element strain simulations. (b) Simulated results showing the strain profile along the planes of the QWs. (c) Enlarged view showing strain distributions near the edge of the disk. The scale bar on the right represents the value of the in-plane strain.

QW layers, based on a model containing four-pairs of 192 nm-disk-shaped QWs as illustrated in Fig. 6(a). Cross-sectional view of in-plane strain distribution along the various layers is depicted in Fig. 6(b), revealing that a higher degree of relaxation occurs towards the disk edges, while the central region remains strongly strained. Similar degrees of relaxation occur at the edges independent of pillar diameters. Fig. 6(c) shows a high-resolution close-up strain map of the sidewall region; the extent of compressive strain gradually increases over a distance of ~20 nm from the edge before attaining its maximum value. Consequently, the observed blue-shift of spectral peaks suggests that a significant proportion of EL signals originate from the strain-relaxed region surrounding the nano-pillars.

In summary, an InGaN LED with an embedded PhC is demonstrated. The PhC is fabricated by etching through an NSL pattern, followed by ELO regrowth. The optical performances of the PhC LEDs have been studied and compared with FDTD simulation results. The periodic ordered nano-pillar structure not only promotes light extraction but also partially suppresses the piezoelectric field through strain relaxation of the InGaN/GaN QWs, supported with μ-Raman spectroscopy spectra. The LEDs with embedded PhCs emit as much as 20% more light than the as-grown LED, as well as exhibiting emission wavelengths nearly invariant of injection currents.

This work was supported by a GRF grant of the Research Grant Council of Hong Kong (Project No. HKU 7117/11E).

[1]T. Takeuchi, S. Sota, M. Katsuragawa, M. Komori, H. Takeuchi, H. Amano, and I. Akasaki, Jpn. J. Appl. Phys., Part 2 **36**, L382 (1997).
[2]A. David, T. Fujii, R. Sharma, K. McGroddy, S. Nakamura, S. P. DenBaars, E. L. Hu, C. Weisbuch, and H. Benisty, Appl. Phys. Lett. **88**, 061124 (2006).
[3]T. Nishida, H. Saito, and N. Kobayashi, Appl. Phys. Lett. **79**, 711 (2001).
[4]T. Fujii, Y. Gao, R. Sharma, E. L. Hu, S. P. DenBaars, and S. Nakamura, Appl. Phys. Lett. **84**, 855 (2004).
[5]H. W. Choi, M. D. Dawson, P. R. Edwards, and R. W. Martin, Appl. Phys. Lett. **83**, 4483 (2003).
[6]C. C. Kao, H. C. Kuo, H. W. Huang, J. T. Chu, Y. C. Peng, Y. L. Hsieh, C. Y. Luo, S. C. Wang, C. C. Yu, and C. F. Lin, IEEE Photon. Technol. Lett. **17**, 19 (2005).
[7]J. J. Wierer, A. David, and M. M. Megens, Nat. Photonics **3**, 163 (2009).
[8]T. N. Oder, K. H. Kim, J. Y. Lin, and H. X. Jiang, Appl. Phys. Lett. **84**, 466 (2004).
[9]S. F. Chichibu, H. Marchand, M. S. Minsky, S. Keller, P. T. Fini, J. P. Ibbetson, S. B. Fleischer, J. S. Speck, J. E. Bowers, E. Hu, U. K. Mishra, S. P. DenBaars, T. Deguchi, T. Sota, and S. Nakamura, Appl. Phys. Lett. **74**, 1460 (1999).
[10]K. H. Li and H. W. Choi, J. Appl. Phys. **109**, 023107 (2011).
[11]C. Wiesmann, K. Bergenek, N. Linder, and U. T. Schwarz, Laser Photonics Rev. **3**, 262 (2009).
[12]C. Kisielowski, J. Krüger, S. Ruvimov, T. Suski, J. W. Ager III, E. Jones, Z. Liliental-Weber, M. Rubin, E. R. Weber, M. D. Bremser, and R. F. Davis, Phys. Rev. B **54**, 17745 (1996).